ELSEVIER

Journal of Alloys and Compounds 305 (2000) 225–238

Journal of ALLOYS AND COMPOUNDS

www.elsevier.com/locate/jallcom

Structure and properties of nanocrystalline TiC full-density bulk alloy consolidated from mechanically reacted powders

M. Sherif El-Eskandarany*

Mining, Metallurgy and Petroleum Engineering Department, Faculty of Engineering, Al Azhar University, Nasr City, 1337 Cairo, Egypt

Received 30 November 1999; accepted 11 January 2000

Abstract

High-energy ball milling has been successfully employed for synthesizing nanocrystalline powders of $Ti_{44}C_{56}$. The milling procedure involves milling of elemental Ti and C powders at room temperature in an argon gas atmosphere. The progress of the mechanically induced solid state reaction was monitored by means of X-ray diffraction, scanning electron microscopy and transmission electron microscopy and/or high resolution transmission electron microscopy at several stages of the milling time. A single phase of NaCl-type TiC is obtained after 22 ks of milling time. No free Ti and/or C crystals could be detected at this stage of milling. Increasing the milling time leads to a decrease in the grain size of the powders to <50 nm in diameter after 40 ks of milling time. Towards the end of the milling processing time (720 ks) the powders possess excellent morphological characteristics, such as a homogeneous shape (spherical-like morphology) with fine and smooth surface relief and uniform size (<1 μm in diameter). The lattice parameter of this end-product was calculated to be 0.4326 nm. In addition, the powders at this final stage of milling consist of nanocrystalline grains (<5 nm in diameter) with cell-like morphology. In order to determine some physical and mechanical properties of the synthesized TiC material, different samples at different milling times were consolidated into bulk samples, using a plasma activated sintering method. The powders of the final-product (720 ks) has a density of 5.21 g/cm^3, being nearly the theoretical density of TiC. In addition, this bulk sample maintains its unique structure characteristics with nanocrystalline grains of <60 nm in diameter. On the basis of the results of the present study, the ball-milling technique accompanied with plasma activated sintering can provide powerful tools for the fabrication of nanocrystalline TiC bulk alloys with unique and advanced properties.

Keywords: Nanocrystalline materials; Carbides; Refractory materials; Ball milling; Powder metallurgy; Density consolidation; Nondestructive testing; Elastic modulii; Hardness

1. Introduction

Due to their unique properties, nonequilibrium materials (amorphous, quasicrystals, solid solutions and nanocrystalline materials) have recently found a wide range of industrial applications. Nanocrystalline materials (also known as nanostructured) [1] which are defined as materials with grain sizes <100 nm, have received much attention as advanced engineering materials with improved physical and mechanical properties [2]. This class of unique materials has been prepared by several techniques, including inert gas condensation [3], rapid solidification [4], electrodeposition [5], sputtering [6], crystallization of amorphous phases [7] and chemical processing [8]. Mechanical alloying (MA) [9] which is a well known process for preparing homogeneous composite particles with intimately dispersed uniform internal structure [10] and several amorphous alloys [11–17], has been considered a powerful technique for synthesizing numerous nanocrystalline materials of pure metals nitrides [18,19], carbides [20–22], composites [23,24], nanocomposites [25,26] and solid solutions [27,28] because it is simple and relatively inexpensive [29]. Carbides, especially those of the transition metals of groups IV and V in the periodic table, possess unusual properties that make them desirable and useful engineering materials for many industrial applications [30]. The cubic form of TiC (NaCl structure) with its extremely high melting point (3373 K) is a refractory material having some of the characteristic properties of metals (luster, metallic conductivity, etc.). In addition, it has extraordinary hardness and toughness, excellent resistance to wear and abrasion and infusibility. TiC has received much attention due to its usage as a hard coating to protect the surface of cutting tools from wear and

*Fax: +20-2-260-1706.

E-mail address: msherif@mst1.mist.com.eg (M. Sherif El-Eskandarany)

0925-8388/00/$ – see front matter
PII: S0925-8388(00)00692-7

Table 1
Possible methods for fabrication of TiC via the technique of powder metallurgy[a]

Method	Reaction
Direct reaction between metallic Ti or metallic Ti hydrides and graphite, under vacuum or inert gas	$Ti+C \rightarrow TiC$ $TiH_2+C \rightarrow TiC+H_2$
Reduction of the Ti oxide by graphite, under vacuum or inert gas	$TiO_2+3C \rightarrow TiC+2CO$
Reaction of the Ti with carburizing gas	$Ti+C_nH_{1-n} \rightarrow TiC+H_2$
Precipitation from the gas phase by reacting the metallic Ti halide or metallic Ti carbonyl in hydrogen	$TiCl_4+C_xH_y+H_2 \rightarrow TiC+HCl+(C_nH_m)$ $Ti+\text{carbonyl}+H_2 \rightarrow TiC+(CO, CO_2, H_2, H_2O)$

[a] After Kieffer and Schwarzkopf (see Ref. [32]).

erosion, extending the tool life [31]. In the industrial scale of production, TiC is prepared at a temperature ranging between 2000 and 2300 K, using the methods that are listed in Table 1 [32]. Considerable attention has recently been paid to another technique for producing TiC using a method called self-propagating high-temperature synthesis (SHS) [33]. For a successful SHS process, the reaction between Ti and C must take place at a temperature higher than the melting point of pure Ti (1843 K) because no reaction can occur below this temperature [34]. The high cost of preparation is a disadvantage of all the previous methods. In this paper, the MA method is proposed for a mechanical carburization solid state reaction between elemental Ti and C powders, which can be successfully achieved in a high-energy ball mill operated at room temperature. The feasibility of employing the MA process for preparing nanocrystalline fcc-TiC powders is demonstrated. The end-product of the milled powders are then consolidated into a fully dense compact, using the plasma activated sintering method. The choice of this consolidation technique comes from the fact that this method is considered as one of the most suitable consolidation processes for preparing nanocrystalline, bulk, fully-dense mechanically reacted materials [18,35]. In spite of the other techniques that are usually used for preparing nanocrystalline materials, the MA method can be easily scaled up to produce larger quantities of several kilograms, using larger types of mills, e.g. low energy ball or rod mills [36,37].

2. Experimental

Pure (99.9%) elemental Ti (30 μm) and carbon powders (5 μm) were used as the starting reactant materials and mixed to give the desired average composition of $Ti_{44}C_{56}$ and then sealed in a sapphire vial (80 ml in volume) together with sapphire balls (10 mm in diameter) in a glove box under an Ar atmosphere. The ball-to-powder weight ratio was 10:1. The milling process was carried out at room temperature using high energy ball mill (Laboratory Centrifuge Mill, P6, Germany). The ball-milling experiments were interrupted after selected milling times and a small amount of the powder was taken from the vial in the glove box. An individual MA experiment was carried out in order to determine the milling temperature during the solid state reaction between the diffusion couples of Ti and C. This was achieved by fixing the end of a thermocouple at the outermost surface of the vial. The ball mill was then operated without any interruptions and the temperatures of the vial were recorded after selected milling times. X-ray diffraction (XRD) with CuKα radiation, transmission electron microscopy (TEM) operated at 200 kV, were used to monitor the structural changes of the powders after several ball milling periods. However, some samples were characterized by high-resolution transmission electron microscopy (HRTEM) operated at 200 kV. The samples of the TEM and/or HRTEM were prepared by mixing the powders with a small amount of pure alcohol (2 ml in volume) and stirring for 30 s. Two or three drops of the suspension were dropped on a Cu-microgrid and then well dried for about 1.8 ks before mounting the microgrid onto the TEM sample holder. The morphological (shape and size) changes of the powder after selected milling times were determined by scanning electron microscopy (SEM) operated at 20–30 kV and an optical microscope. In order to determine the Ti content and the contamination degree of Al (that might be introduced to the milled powders on using the sapphire milling tools), the powders of the final product (720 ks) were analyzed by the induction coupled plasma emission method. On the other hand, the concentration of C, and the contamination content of oxygen that is introduced into the powders during the milling procedure and/or during the powder handling outside the glove box, were determined by the helium carrier fusion-thermal conductivity method.

The mechanically reacted powders were then consolidated in vacuum at 1963 K under pressure ranging from 19.6 to 38.2 MPa for 0.3 ks, using a plasma activated sintering (PAS) method. In order to avoid undesired grain growth, the sintering process was applied for only 0.18 ks. No binding material was used in this consolidation pro-

Table 2
Chemical analyses of as-milled and as-consolidated mechanically reacted TiC after 720 ks of ball milling time

Sample	Ti content (at.%)	C content (at.%)	Al content (at.%)	O content (at.%)
As-milled	44.80	54.93	0.03	0.24
As-consolidated	44.45	55.17	0.03	0.35

cedure. The as-consolidated samples were also characterized by means of XRD, TEM, SEM and chemical analyses, using the same experimental conditions as mentioned above. Selected samples (the end-product) were investigated by HRTEM. The density of the consolidated TiC was determined by Archimedes' principle using water immersion. A Vickers indenter with a load of 50 kg was used to determine the hardness of the compacted samples that were milled for selected MA times. The hardness values reported below (Section 3) are averaged from ten indentation results. In addition, some mechanical properties of the consolidated samples were determined by non-destructive tests.

Table 2 shows the chemical analyses of the as-milled and as-consolidated samples of TiC. Obviously, the as-sintered sample takes up 0.10 at.% oxygen during the consolidation procedure, although, the sintering was achieved under high vacuum, as high as 6.0×10^{-6} torr. This may be attributed to some leaks in the vacuum system of the PAS. Nevertheless, the total contamination content of the bulk sample is 0.38 at.%, being acceptable for several industrial applications.

3. Results

3.1. Formation of TiC powders by mechanical alloying

3.1.1. Structural changes with milling time

The XRD patterns of ball-milled $Ti_{44}C_{56}$ powders are presented in Fig. 1 after selected MA times. After 2 ks (Fig. 1a), the powders are mixtures of the starting reactant materials, characterized by the sharp Bragg peaks of elemental Ti and C. Increasing the MA time (6–8 ks) leads to a remarkable decrease in the intensity of the Bragg peaks for pure graphite crystals (Fig. 1b–c) that can be hardly seen after 11 ks of the MA time (Fig. 1d). This is attributed to a solid state diffusion of the C atoms that have small atomic radii into the lattice of hcp-Ti. Moreover, the Bragg peaks for pure Ti crystals shifted to the low angle side, suggesting the formation of an interstitial hcp-TiC solid solution (Fig. 1d). After 15 ks of MA time (Fig. 1e), a new phase corresponding to NaCl-TiC is formed, characterized by the Bragg peaks of TiC (111), TiC (200), TiC (220), TiC (311) and TiC (222) reflections. After 22 ks of the MA time, the Bragg peaks of the reactant materials (Ti

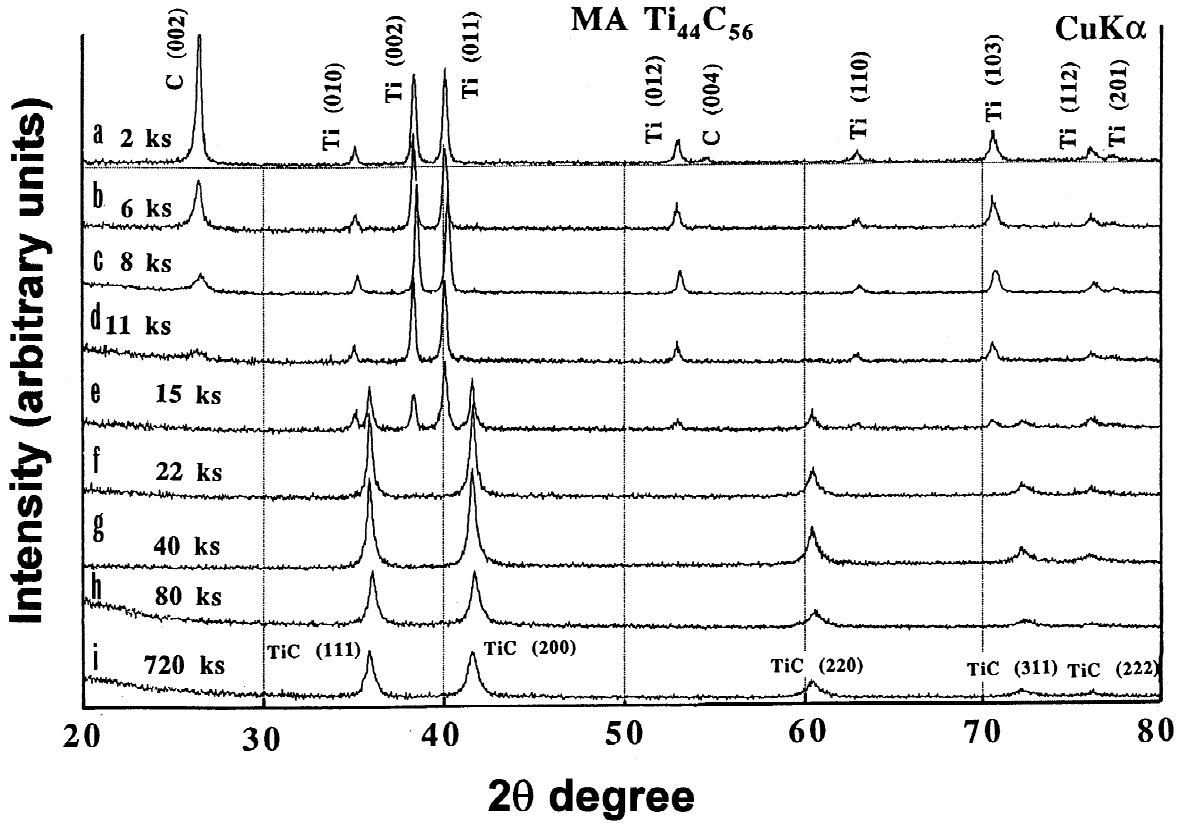

Fig. 1. XRD patterns of mechanically alloyed $Ti_{44}C_{56}$ powders after selected MA times.

and graphite) surprisingly disappeared and the reflections from the TiC crystals become sharp and pronounced, indicating the completion of the MA process (Fig. 1f).

The lattice parameter (a_0) of the formed phase for TiC was calculated after 40 ks (Fig. 1g) of the MA time and found to be 0.4326 nm, in a good agreement with the reported value (0.4327 nm) [38]. It is worth noting that the intensity ratio of these Bragg peaks are almost in good agreement with those of the TiC powder [38], suggesting that the crystal structure of the obtained powders is of the NaCl type. Increasing the MA time to 80 ks (Fig. 1h) leads to an increasing mechanical deformation that is generated by the milling tools, causing a remarkable decrease in the grain size of the powders, suggested by the broadening of the Bragg peaks at this stage of milling. Further milling (720 ks) leads to the formation of nanocrystalline TiC, indicated by very broad Bragg peaks, as shown in Fig. 1i. This phase of TiC does not transform to any other phase(s) even after longer milling times, as long as 1000 ks.

Detailed TEM analyses were performed in order to understand the local structure changes of the mechanically reacted powders during the various stages of the MA process. The HRTEM micrograph of the powders that were milled for 2 ks of the MA time is shown in Fig. 2. The powders are mixtures of pure graphite (extended thin veins) and the matrix of Ti (dark area). The lattice fringe spacing in Fig. 2b is measured to be 0.335 nm, which matches with the plane (002) of carbon (0.338 nm). The existence of the TiC phase could not be detected at this stage of milling, and the powders are typical Ti–C composite particles, containing thin veins ($<$10 nm in thickness) of C layers embedded in the soft matrix of Ti. A mechanical solid state reaction takes place at the interfaces of these fresh layers and a new phase of TiC results after further milling.

Fig. 3 shows the bright field image (BFI) of the powders that were milled for 15 ks of MA time. The structure of the particle is fine. However, several faults and defects such as twins and nanotwins are observed. The presented BFI is classified into three zones, i.e., I, II and III and the corresponding selected area diffraction patterns (SADPs) (Fig. 3b–d) are shown in the inset of the micrograph. At this stage of milling, the powders differ widely in the internal structure from region to region, displaying a heterogeneous structure. The SADP presented in Fig. 3b (corresponding to zone I), consists of sharp rings that correspond to the coarse fcc-TiC grains (the obtained product), coexisting with unprocessed hcp-Ti (sharp spots). Zone II is a TiC-rich region, that coexisted with small mole fractions of unprocessed Ti crystals (sharp spot patterns), as shown in Fig. 3c. Zone III, however, shows the existence of a single phase of fcc-TiC (Fig. 3d).

The BFI and the corresponding SADP of the powders which were milled for 40 ks, are shown together in Fig. 4. Overall, the sample consists of rather coarse lenses or cells

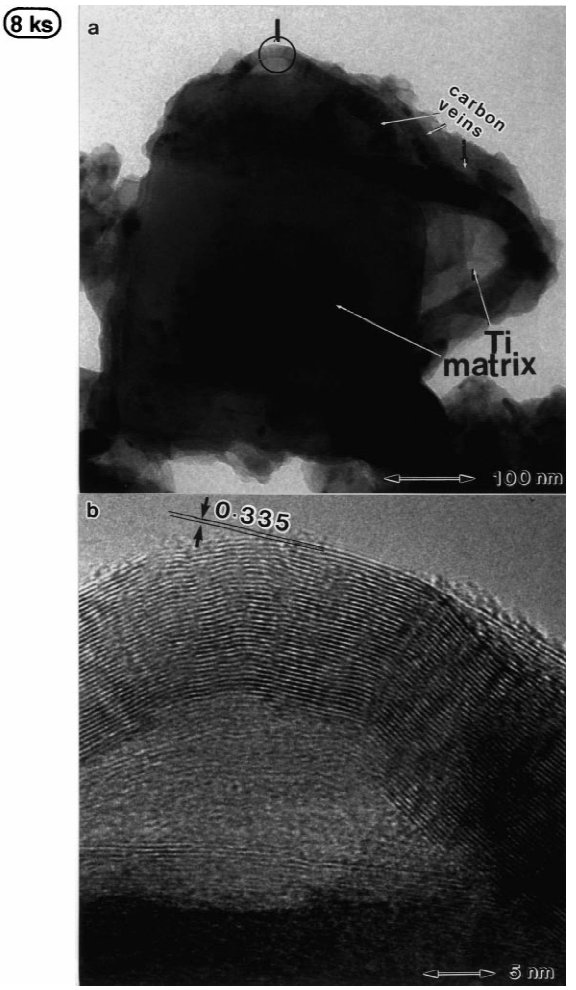

Fig. 2. (a) Low magnification HRTEM image of the milled powders after 2 ks of MA time, and (b) enlarged micrograph of region I which is marked in (a). The lattice fringe spacing in (b) is measured to be 0.335 nm, matching with the plane (002) of carbon (0.338 nm [38]).

with wide size distribution, ranging from 20 to 60 nm (Fig. 4a). Remarkably, a single phase of NaCl-type TiC is detected, characterized by the Debye–Scherrer rings corresponding to TiC, as indicated in Fig. 4. No free Ti and/or C crystals could be observed after this stage of milling.

After 80 ks of the MA time, the powders have nanocrystalline spherical grains of about 4 nm (or less) (Fig. 5a) in diameter. The indexed SADP still shows clear fcc rings of the obtained TiC (Fig. 5b). The absence of the spots in the SADP indicates the formation of fine grains TiC powders.

The HRTEM image of the final product for TiC that was ball-milled for 720 ks of the MA time, is presented in Fig. 6. HRTEM observations show the lattice fringe image of TiC alloy. This lattice fringe spacing was measured to be about 0.250 nm, which matches the interplanar spacing of TiC (111) [38].

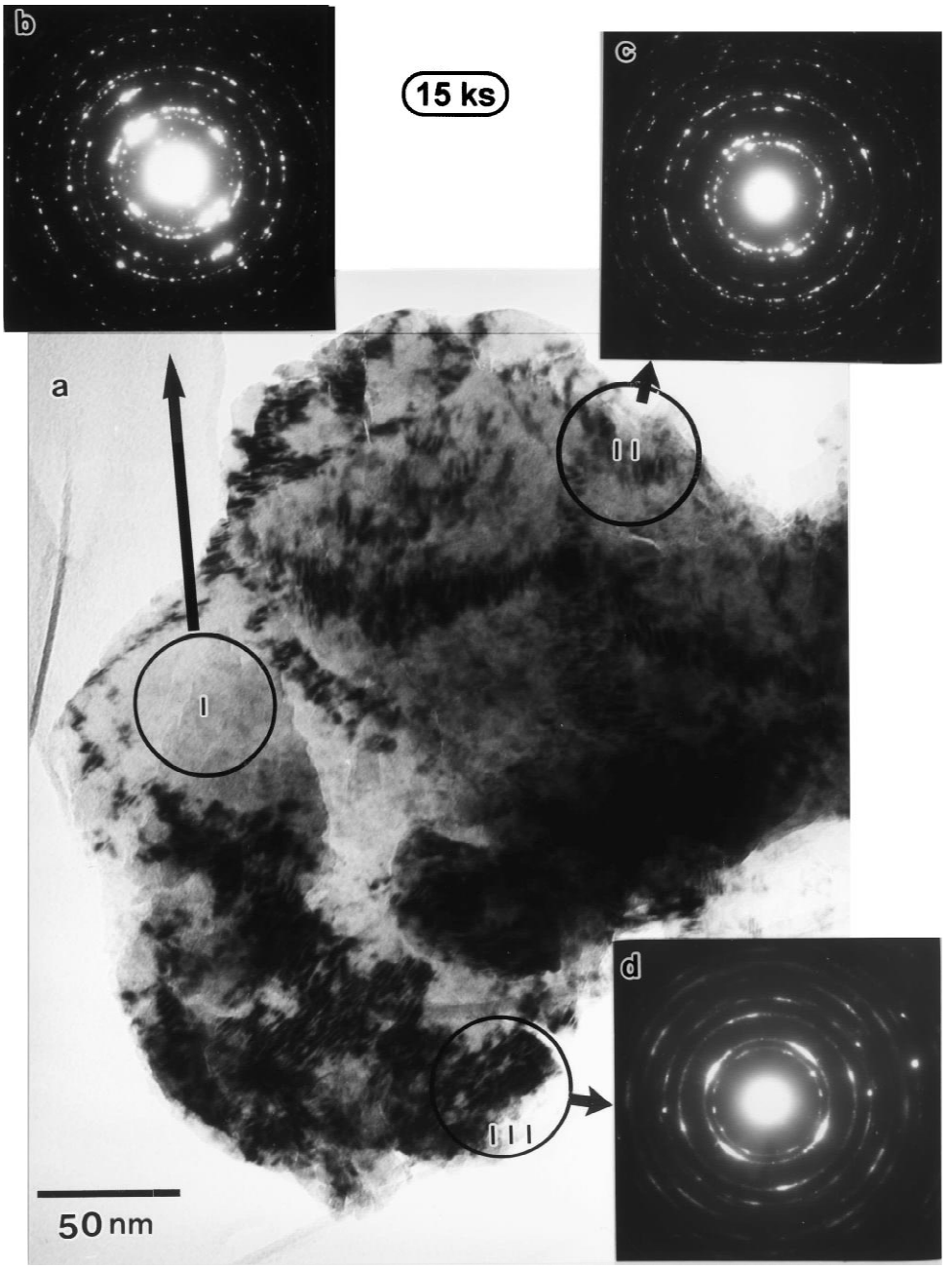

Fig. 3. (a) BFI and the corresponding (b, c, d) SADPs of a mechanically alloyed sample after milling for 15 ks. The sample differs widely in structure within the particle itself.

3.1.2. Morphology changes with milling time

SEM was used to follow the changes in the shape and size of the milled powders during the different stages of the MA process. Fig. 7 shows the SEM micrographs of the starting material powders (0 ks of the MA time) of Ti (Fig. 7a) and C (Fig. 7b). The powders of the reactant materials are bulky with random shape and size. During the early stage of milling (11 ks), the powders tend to agglomerate and form large composite Ti–C particles of about 800 μm in diameter (Fig. 8a). The metallographical examinations of the polished and etched particles show that the individual particle contains many thick layers of the diffusion couples of Ti and C powders. Increasing the milling time to 22 ks, enhances the solid state reaction which takes place at the clean interfaces of these layers. The end product of this stage of milling (intermediate) consists of very fine powders with smooth and clean surfaces with an average diameter of about 4 μm (Fig. 8b). Increasing the

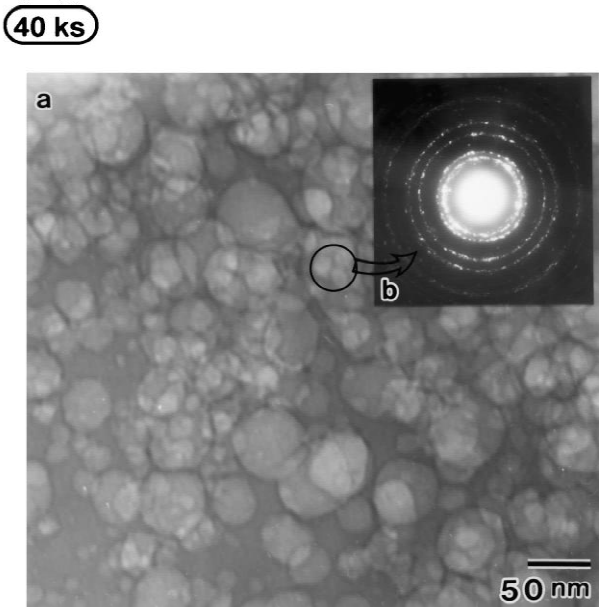

Fig. 4. BFI (a) and the corresponding SADP (b) for the sample that is obtained after 40 ks of MA time. The micrograph shows cell structure morphology with lens-like morphology of about 35 nm in diameter.

milling time to 40 ks (final stage), leads to a remarkable decrease in the size of the TiC powders (0.5–1.5 μm in diameter), causing the formation of uniform spherical-like morphology (Fig. 9a). Towards the end of the MA process (refining stage), the powders possess excellent morphological properties, such as a homogeneous shape with fine and smooth surface relief and uniform size (0.6–0.8 μm in diameter), as shown in Fig. 9b).

3.2. Consolidation of the mechanically alloyed TiC powders

A sintering step using the PSA technique is applied to consolidate the powders after selected MA time. Fig. 10 shows the cross-sectional view of as-consolidated powders that were milled for 15 (Fig. 10a), 40 (Fig. 10b) and 720 ks (Fig. 10c). As was previously presented in the X-ray analysis (Fig. 1e), after 15 ks of the MA time, the as-milled powder consists of two phases: unreacted metallic Ti and fully reacted fcc-TiC. Since the consolidation procedure took place at 1963 K (just above the melting point of Ti (1943 K)) and far below the melting point of TiC (3373 K), the particles of TiC in the mixed powders (the agglomerated particles in the center of Fig. 10a) are embedded in the molten Ti matrix to form composite Ti–TiC compact. Thus, the consolidated samples after this stage of milling are either rich or poor in TiC. During the Vickers hardness measurements, the sample hardness vary from few (nearly 2.5 GPa) to 29 GPa, as shown in Fig. 11.

The microstructure of the consolidated sample for the end product (40 ks) shows a high-density structure with nearly equiaxed grains of about 15 μm in diameter, as

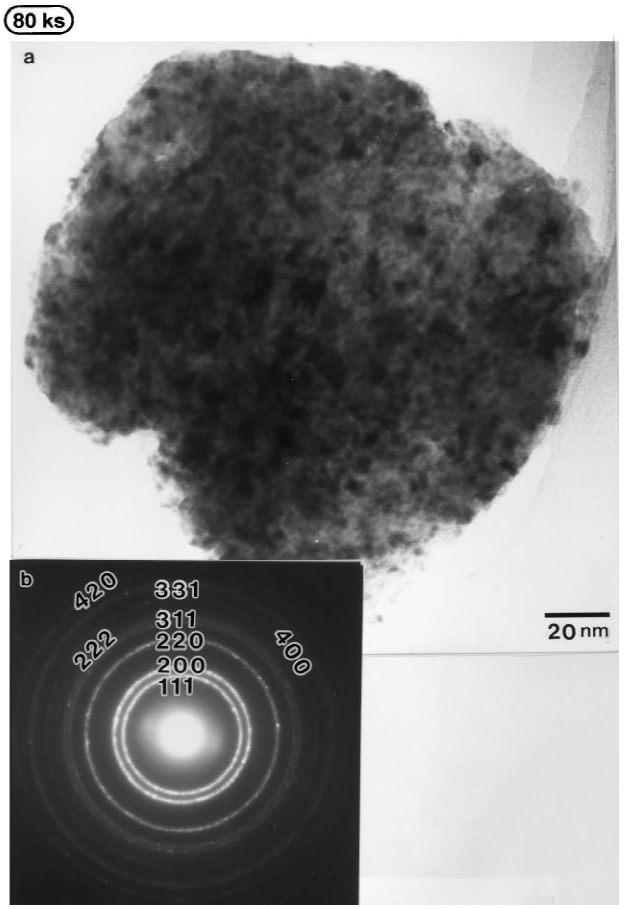

Fig. 5. BFI (a) and the corresponding SADP (b) for the sample at the final stage of MA (80 ks). At this stage of milling, the powders contain nanocrystalline spherical cells of less than 4 nm in diameter (a) with fcc structure corresponding to the TiC phase (b).

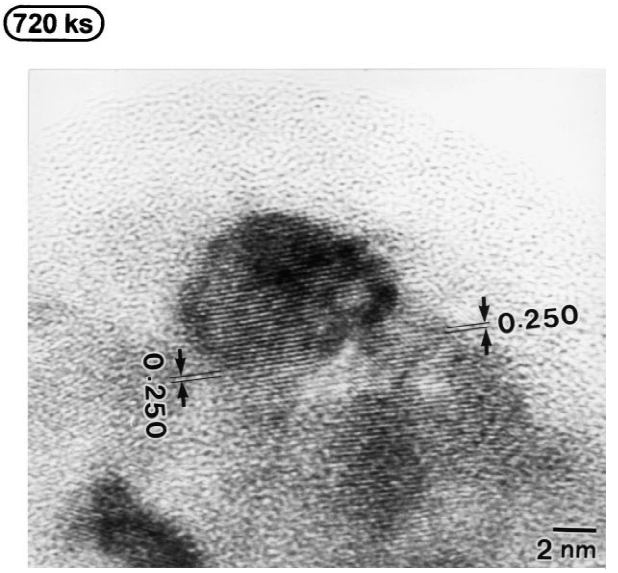

Fig. 6. HRTEM image of the sample at the refining stage of milling (720 ks). The micrograph shows a lattice fringe spacing of 0.250 nm that matches well with the interplanar spacing of TiC (111) [38].

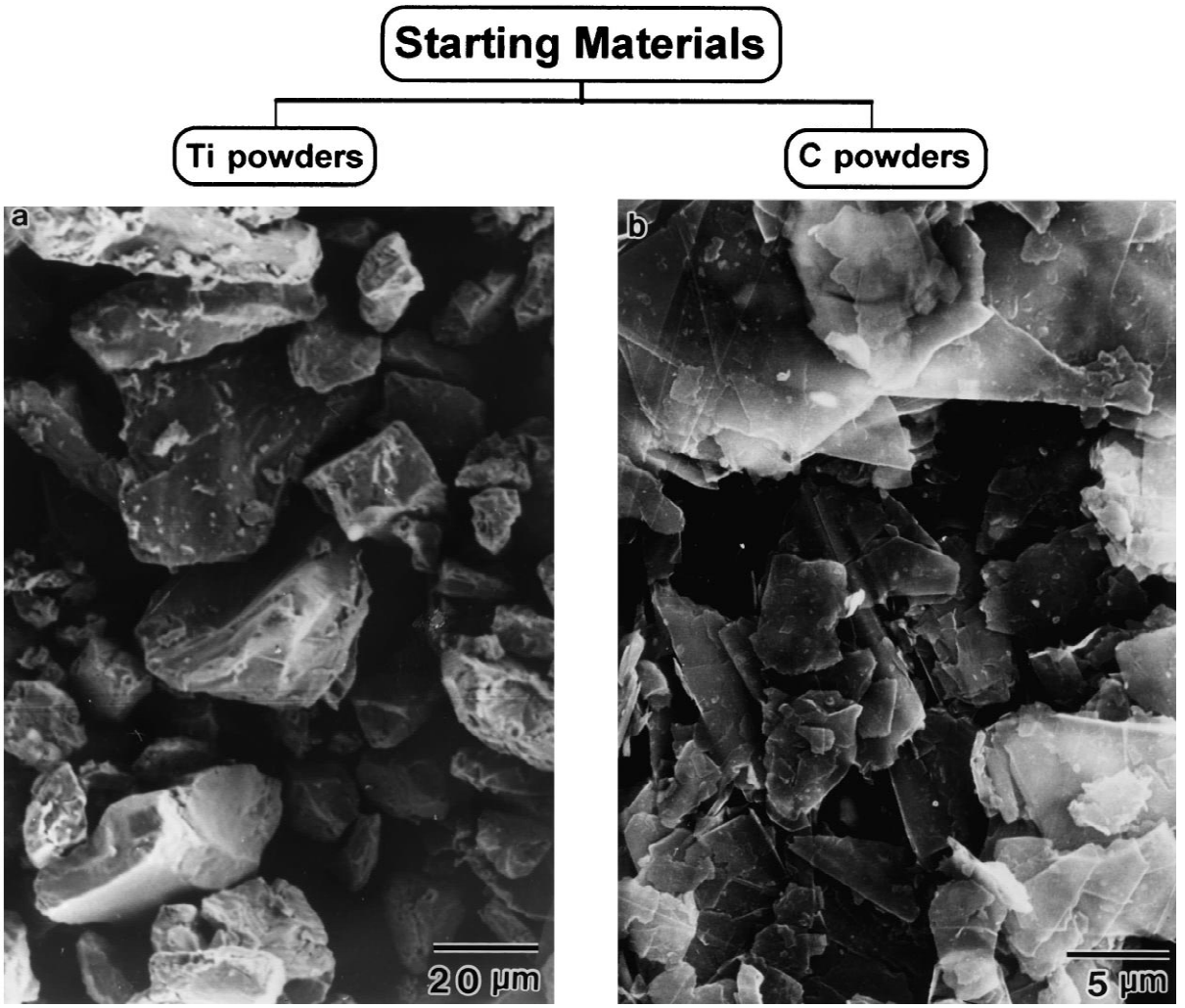

Fig. 7. SEM micrographs of the starting materials (0 ks of MA time) for elemental (a) Ti and (b) C powders. The powders of the reactant materials are bulky with random shape and size.

shown in Fig. 10b. The microstructure of the consolidated powders after the refining stage of MA (720 ks) is composed of fine grains (<5 μm in diameter) and a dense structure, as presented in Fig. 10c. The irregular grain edges in some cases in Fig. 10b and c arise from the long etching time used during the sample preparation.

The BFI and the corresponding SADP of the as-consolidated sample that was milled for 720 ks of MA time, are shown together in Fig. 11. Note the high dense and nanostructure characteristics of the sintered sample. Comparing this micrograph with that in Fig. 5, we can conclude that the consolidation step leads to moderate grain growth. Since the average grain size of this consolidated sample is <100 nm (~60 nm in diameter), one can say that the sintered sample maintains its nanocrystalline character. In addition, this consolidation step does not lead to any structural changes, and the sintered TiC bulk material maintains its fcc structure, as shown by the indexed SADP in Fig. 11b.

The dependence of the hardness of the consolidated TiC samples on the MA time and the grain size, is displayed in Fig. 12. As was previously displayed in Figs. 4 and 5, increasing the MA time leads to refine the grains of the milled powders. At a specific MA time, the grain size of the compact sample depends on the original grain size of the as-milled powders that were used as source for the consolidation procedure. This correlation can be understood from the plot of the grain size for as-milled and as-consolidated samples against the MA time (see Fig. 13). One can conclude that increasing the MA time leads to a decrease in the grain size of the powders and this leads to a marked decrease in the grain size of the sintered samples. Thus, the MA time can play an important role in obtaining nanocrystalline bulk material with improved grain size strengthening (see (Fig. 12). As the grain size of the compacted samples decreased, the Vickers hardness value increased, to about 32 GPa after 720 ks of MA time. The high hardness value of this sample is attributed to the grain boundary hardening effect due to Hall–Petch assumption.

Fig. 14 shows an unetched SEM micrograph (Fig. 14a)

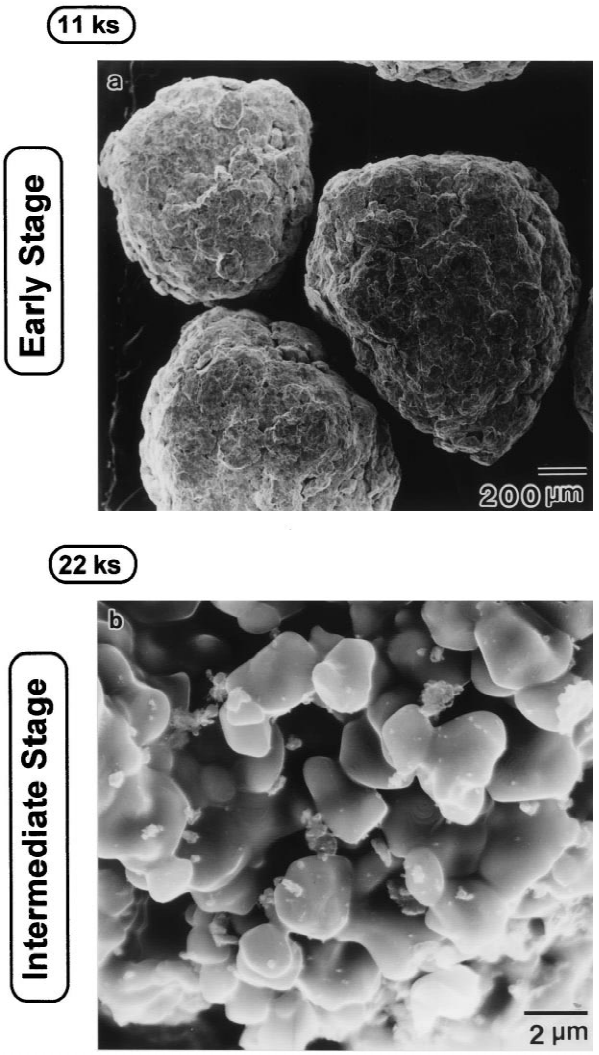

Fig. 8. SEM micrographs of powders of mechanically alloyed TiC at (a) the early stage (11 ks) and (b) the intermediate (22 ks) stages of milling. During the early stage of milling, the powders tend to agglomerate and to form large composite Ti–C particles of about 800 μm in diameter (a). The powders of the intermediate stage of milling (b) consist of very fine particles (about 4 μm in diameter) with smooth and clean surfaces.

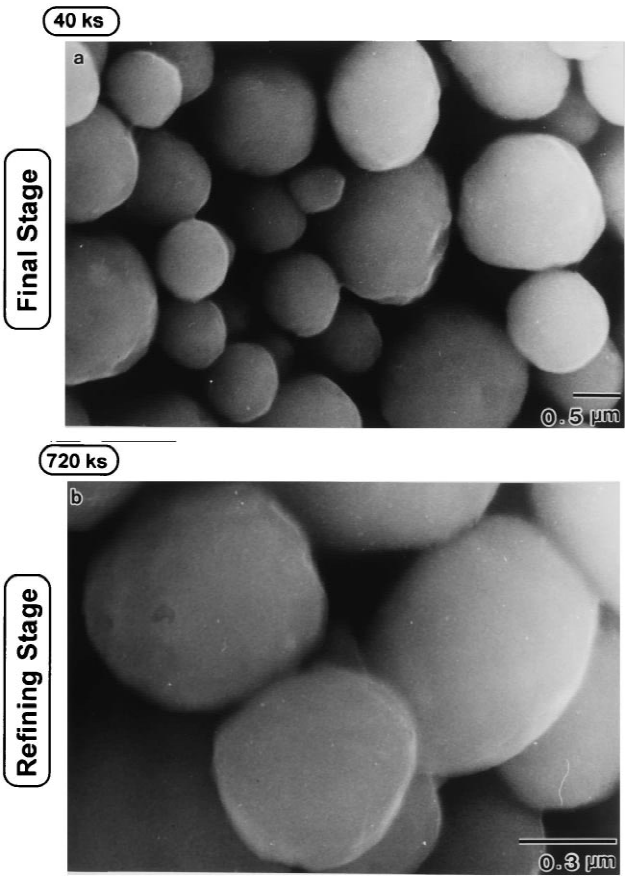

Fig. 9. SEM micrographs of powders of mechanically alloyed TiC at (a) the final stage (40 ks) and (b) the refining (720 ks) stages of milling. The powders at the refining stage of milling (b) possess excellent morphological properties, such as homogeneous shape with fine and smooth surface relief and uniform size (0.6–0.8 μm in diameter).

and the X-ray maps of elemental Ti (Fig. 14b) and C (Fig. 14c) of an as-consolidated sample that was milled for 720 ks of MA time. Obviously, the intensity of the dots corresponding to Ti and C is proportional to their concentration at that particular location. No segregation on a micrometer scale of the elements can be detected and the elements are distributed homogeneously, indicating the formation of single TiC material and the absence of any unprocessed Ti and/or C powders.

The bulk density of the as-consolidated samples is plotted as a function of the MA time in Fig. 15. During the early and the intermediate stages of milling (3–40 ks), the bulk density increases monotonically with increasing MA time, suggesting the existence of the higher density phase (TiC). The portion of the relation between the MA time and the density at the final and the refining stages of the MA (40–720 ks), is presented in a larger scale in the inset of Fig. 15. The densities of the consolidated samples at this stage of milling are increased linearly in the range 5.185–5.210 g/cm^3. This slight increase is may be attributed to grain refining that can play an important role for obtaining higher dense material [39]. Comparing the values of the densities for the samples at the refining stage (5.210 g/cm^3) with the theoretical density of TiC [38] one can deduce that the sintered TiC is fully dense.

Poisson's ratio and the elastic modulii of the consolidated powders were estimated from the measured sample densities and the constant parameters of the nondestructive testing apparatus and are plotted as a function of the MA times in Figs. 16 and 17, respectively. Increasing the MA time leads to an increase in the fraction of TiC vs. that of unreacted Ti. This leads to a monotonic decrease in the value of Poisson's ratio to ≈0.261, after 720 ks of the MA time. This value is smaller than that for unprocessed metallic Ti (0.321), suggesting the formation of a brittle phase of TiC.

The elastic modulii presented by the bulk modulus, Young's modulus and the shear modulus of the consoli-

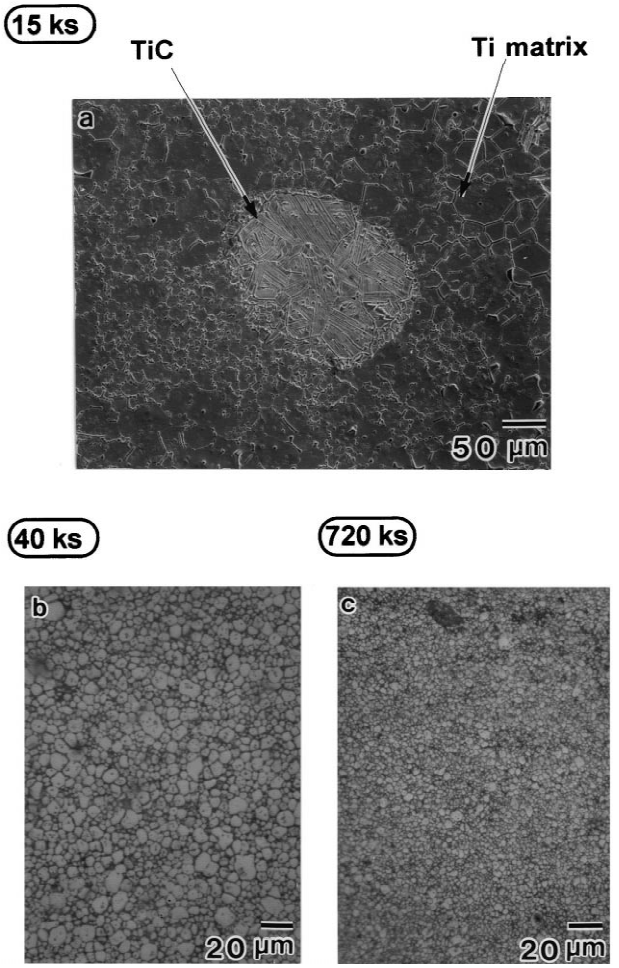

Fig. 10. Cross-sectional views of the as-consolidated powders which were milled for (a) 15 ks, (b) 40 ks and (c) 720 ks of the MA time. During the consolidation of the powders of the early stage of milling, the TiC particles are embedded in the molten Ti matrix to form composite Ti–TiC compacts (a). The micrographs of the final and refining stages reveal fine structure of a single phase of TiC.

dated mechanically reacted TiC powders are shown as a function of the MA time in Fig. 17. These values increase significantly during the early and intermediate stages of milling (0–40 ks), suggesting an increase of the TiC in the milled powders. Towards the end of the MA process (40–720 ks), the values of the elastic modulii are almost saturated or slightly increased, indicating the formation of a single homogeneous phase of TiC.

4. Discussion

Although all the TiC alloys are usually prepared by direct union of the elements by heating the metal in the vapor of a suitable hydrocarbon, synthesizing TiC by mechanical solid state reaction via the ball milling technique has received much attention. This is attributed to the simplicity of the technique and the large amounts of

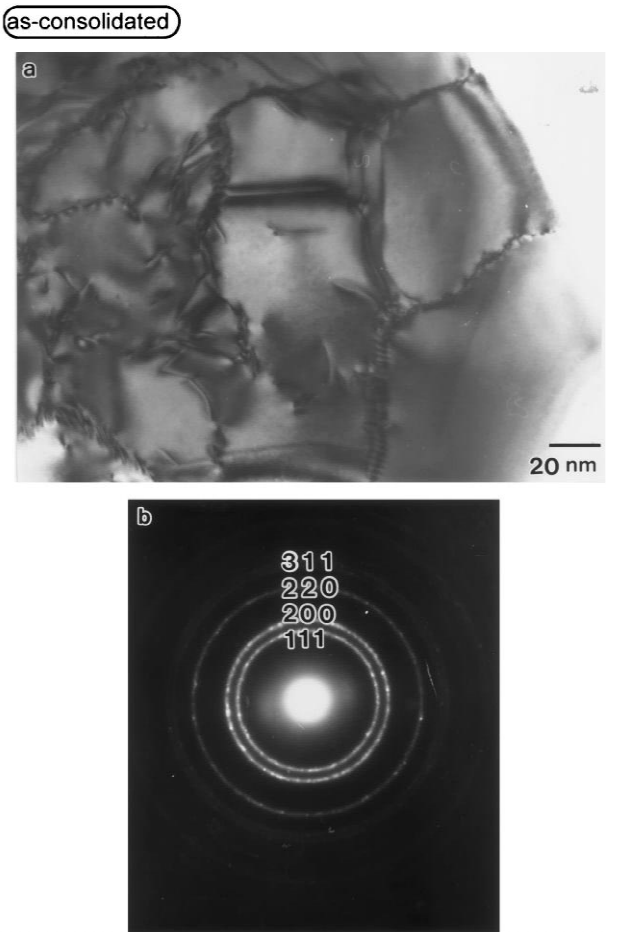

Fig. 11. (a) BFI and (b) the corresponding SADP of the as-consolidated TiC powders after milling for 720 ks. Note the high dense and the nanostructure characteristics of the sintered sample.

homogeneous powders that can be obtained on an industrial scale at room temperature.

In fact, TiC formation is a typical exothermic reaction with a large negative heat of formation (−77 kJ/mol) [40]. Based on the results of the present study, $Ti_{44}C_{56}$ can be

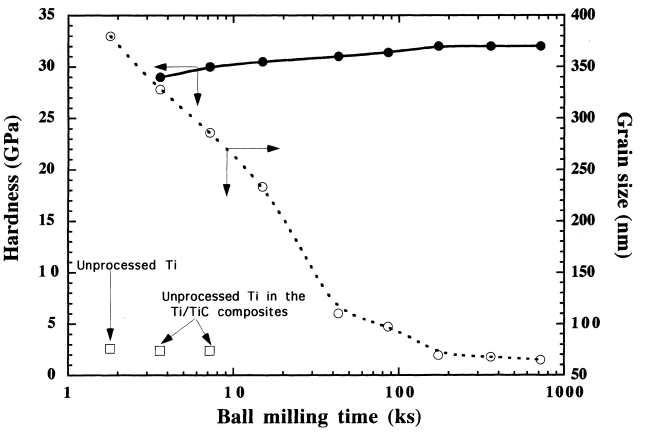

Fig. 12. Correlation between hardness, grain size and MA time for as-consolidated TiC bulk alloys.

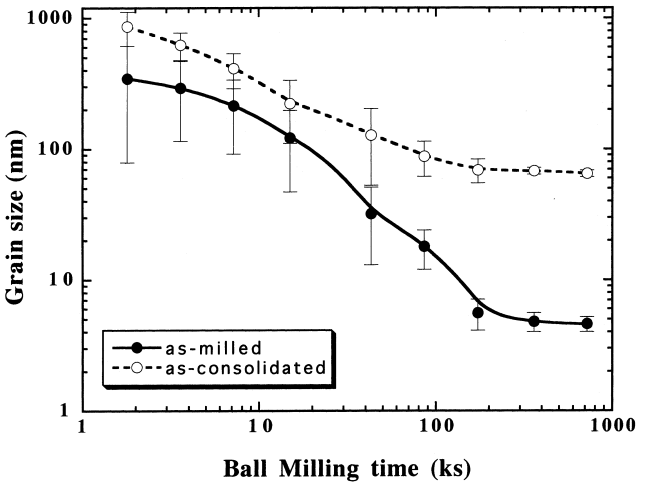

Fig. 13. Dependence of the grain size of the as-milled (solid line) and as-consolidated (broken line) on MA time.

obtained by high-energy ball milling of elemental Ti and graphite powders at room temperature. Neither solid solution nor amorphous phases could be detected at the end stage of the milling process. In this section, the mechanism for formation of TiC alloy powders by MA method will be discussed. In addition, the consolidation of the product powders into nanocrystalline compacts is explained as well.

4.1. Formation of TiC powders by mechanical alloying

Fig. 18 presents the dependence of the vial temperature on the MA time. We should emphasize that the measured temperature here cannot be used to tell us the actual temperature that occurs at the ball–powder–ball collision or the heat liberated during the reaction of Ti with C. This is because the actual temperature decreases when going from the reaction zones in the innermost portion of the vial to outermost surface of the vial. Hence, the measured temperature here can just be used to express the kinetics of the reaction during the various stages of milling. These experiments were achieved using an agate vial containing the milling charge of reactant materials of Ti and C powders together with the milling media (the agate balls). The data were obtained by fixing the end of a thermocouple at the outermost surface of the vial; the ball mill was then operated without any interruptions. The temperatures of the vial were recorded at selected MA times (solid line). In order to observe the relative temperature rise during the reaction, the same experiments were achieved using the same vial but containing the milling media only (broken line). Obviously the temperature of the vial that contains the milling media only monotonically increases with increasing milling time to reach a value of 315 K after 9 ks of milling time. No marked change in this value could be

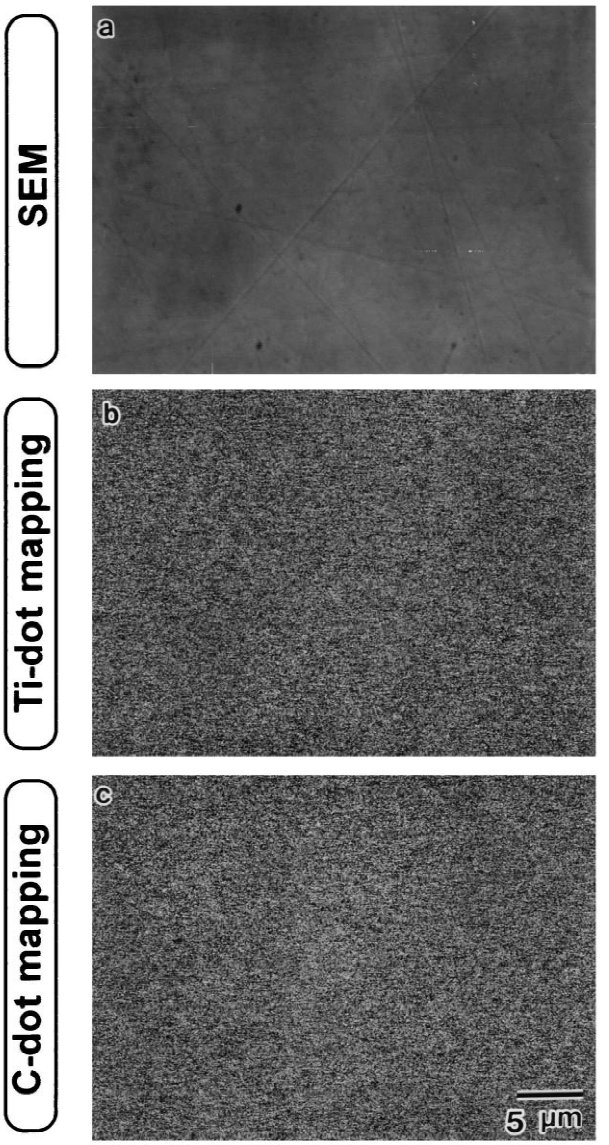

Fig. 14. SEM micrograph (a) and dot mapping of Ti (b) and C (c) of the as-consolidated mechanically alloyed TiC after 720 ks of MA time. The intensity of the dots corresponding to particular Ti and C is proportional to their concentration at that particular location, indicating the formation of a single uniform phase of TiC.

observed even after longer milling time (1000 ks). The situation differs when the ball mill contains both the balls and the reactant materials. In this case, the vial temperature increased monotonically during the first few kiloseconds of milling (0–9 ks). During the second stage of milling (9–5 ks), however, the temperature dramatically increased to reach a maximum value of 332 K after 15 ks of MA time. During this early stage of milling the powder particles of Ti and C are blended together and grow in size to form composite particles (Fig. 2) of a larger diameter (~ 800 μm) as a result of cold welding (Fig. 8a). A partial reaction between the reactant powders takes place, and a small

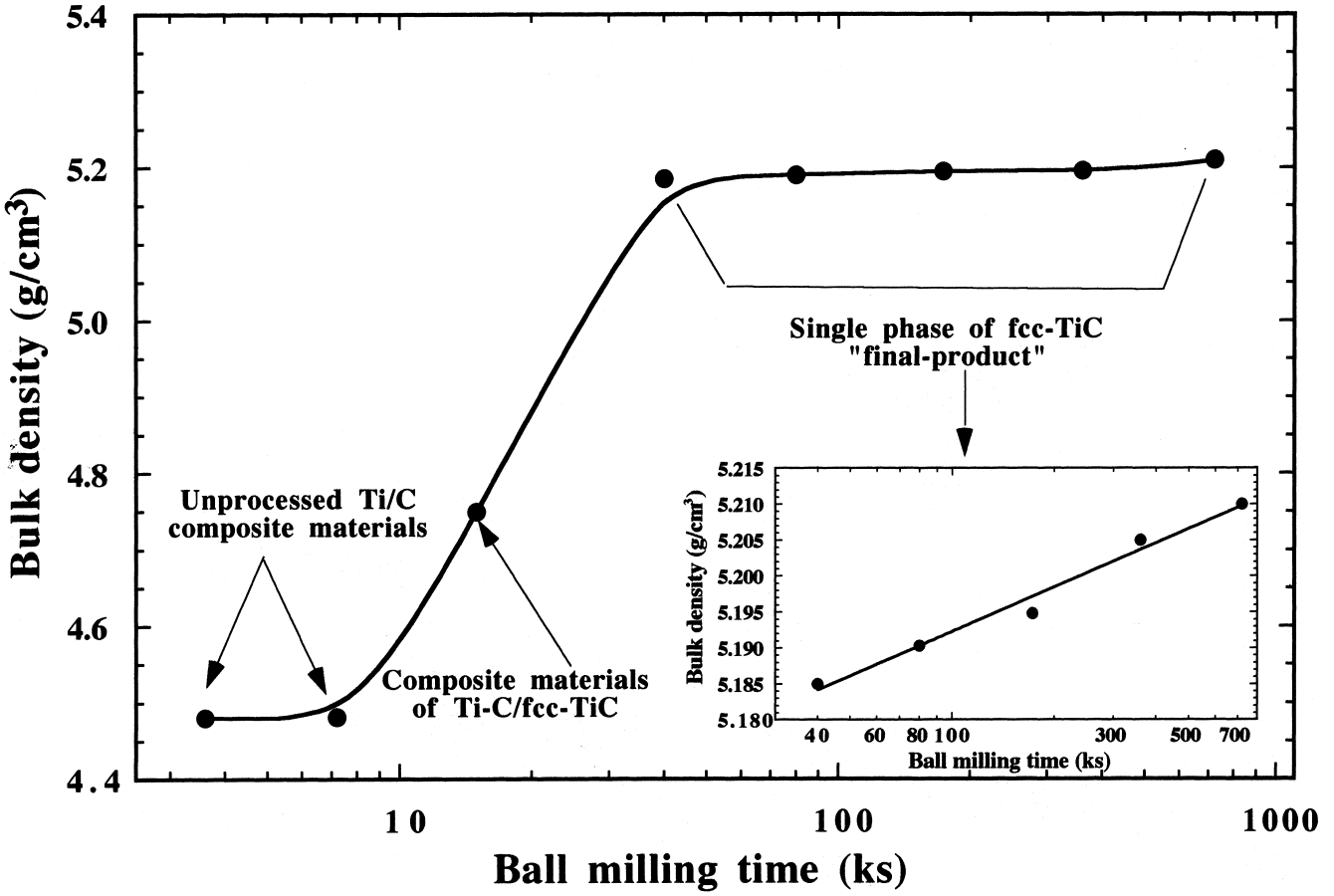

Fig. 15. Correlation between the bulk density of the consolidated samples and the MA time. The densities vs. the MA time for the as-consolidated samples at the final and refining stages of milling are shown in a different scale in the inset of the figure. The slight increase in the values of the densities (5.185–5.210 g/cm^3) at these two stages of milling, may be attributed to grain refining that can play an important role for obtaining higher dense material [39]. The samples of the refining stage (80–720 ks) are fully dense.

mole fraction of TiC is formed after 11 ks of milling (Fig. 1d). At this stage, a mechanical solid state reaction starts and considerable amounts of the product (TiC) are formed.

The previous stage of milling is followed by a second stage (14–40 ks) in which a complete solid state reaction takes place between the diffusion couples of Ti and C in the composite particles and a new phase of NaCl–$Ti_{44}C_{56}$ is formed. Here, all the reactant materials have already reacted completely, and a single phase of TiC is formed after about 22 ks (Fig. 1f). During this stage of milling, the vial temperature increased to be about 342 K (Fig. 18). This reaction is accompanied by the evolution of heat. Thus, the heat liberated on reacting Ti with C, which is transferred to the surface of the vial, is measured to be 28 K (net temperature). The net temperature of the vial during this stage equals the difference between the temperature of the vial when it contains the milling charge of the balls and the powders and the temperature of the vial when it contains the balls only. The temperature of the vial saturated at this value for an MA time of 40 ks, as displayed in Fig. 18.

After the reaction was completed the temperature of the vial decreased drastically during the disintegration stage (40–54 ks) to reach a minimum value of 328 K after 54 ks of MA time. Once the temperature of the vial has decreased, the powder particles are no longer welded on the surface of the ceramic milling tools so that the powders are moved to the effective zone of the milling media (balls). Thus, a drastic decrease in the particle size could be achieved. During this disintegration stage (40–80 ks), the powder particles have smooth surface relief, spherical-like morphology, and an individual particle size of about 1 μm in diameter (Fig. 9a). In addition, the particles consist of fine cells with an average grain size of about 35 nm in diameter.

During the refining stage of the MA (80–720 ks), a complete homogenization of the powder particles takes place. At this stage of milling, the powders become ultrafine and the size of the individual particles is <0.8 μm in diameter. Moreover, the particle size distribution of the powders has become very narrow, indicating the formation of homogeneous and uniform powder particles (Fig. 9b).

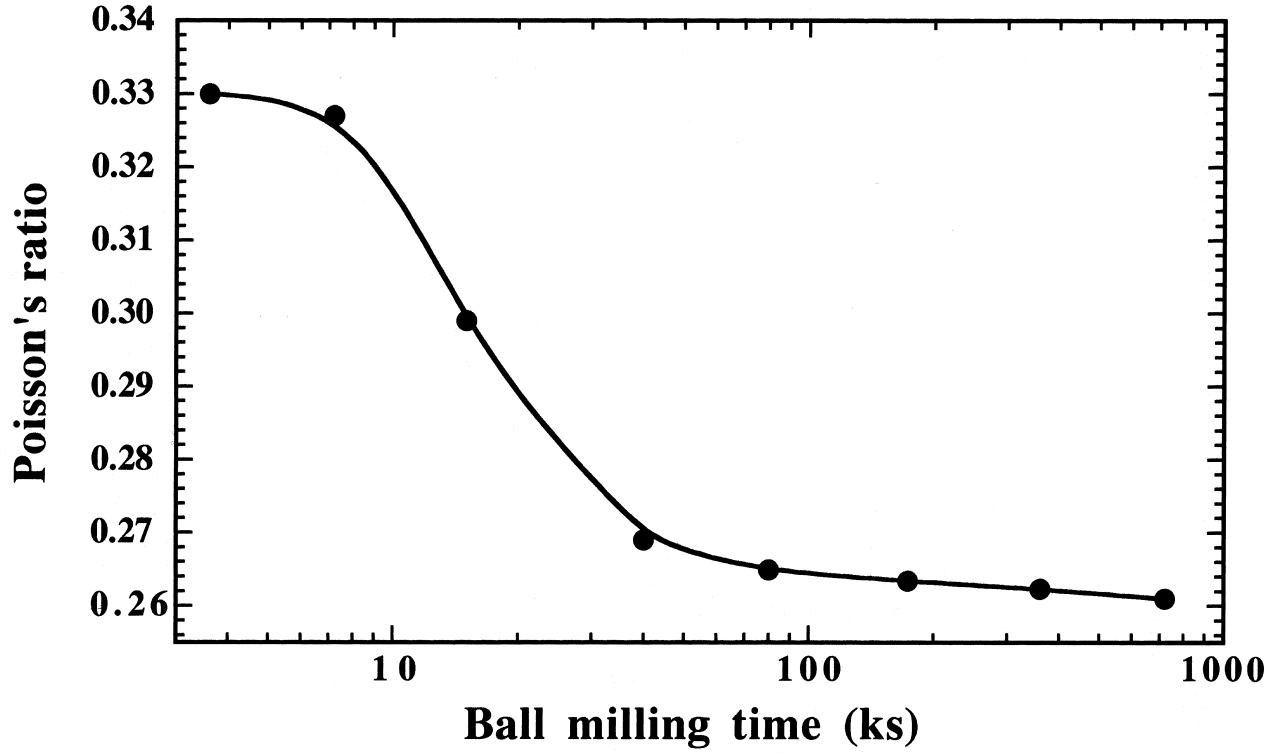

Fig. 16. Dependence of Poisson's ratio of the consolidated powders on MA time. The remarkable decrease of this ratio indicates the progress of the solid state reaction and the increasing of the TiC phase in the milled powders.

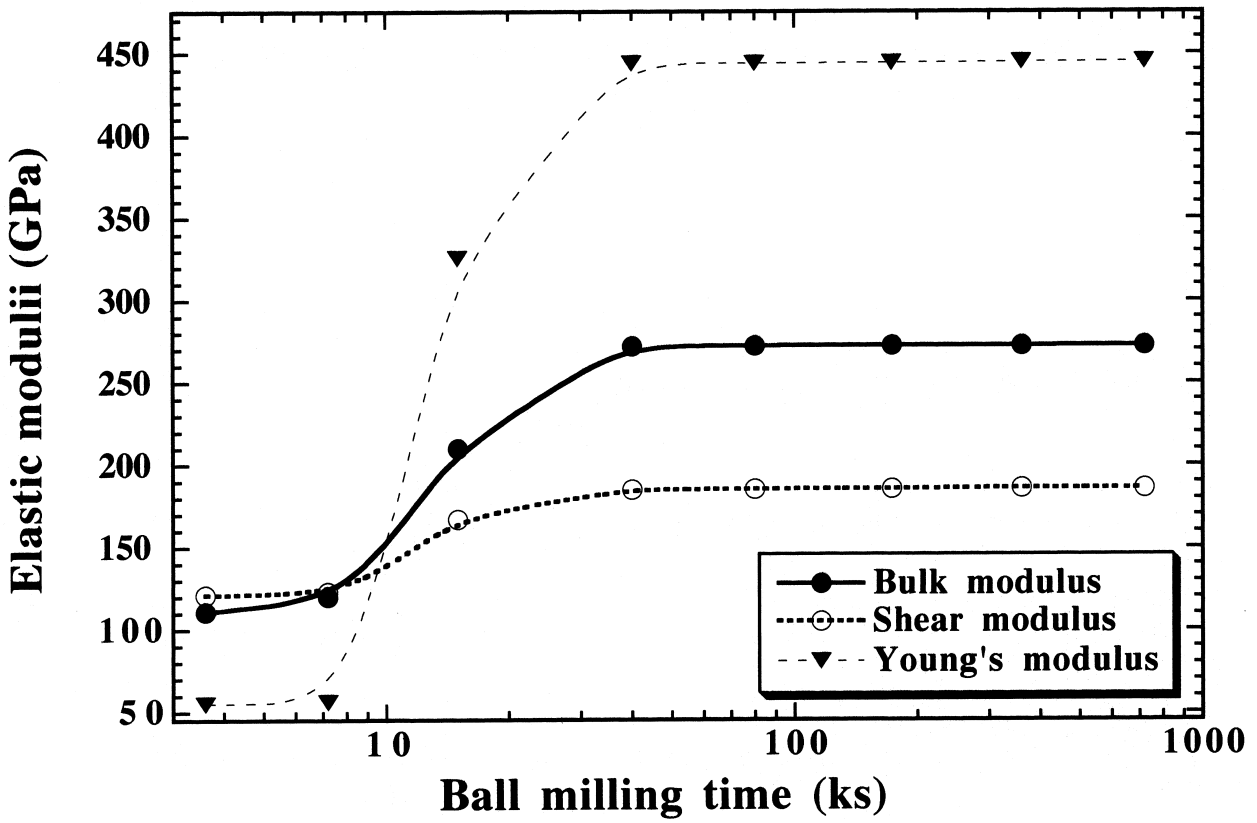

Fig. 17. Relationship between the elastic modulii of the consolidated powders and MA time. The remarkable increase in these values, suggests a monotonical increase of a hard phase of TiC.

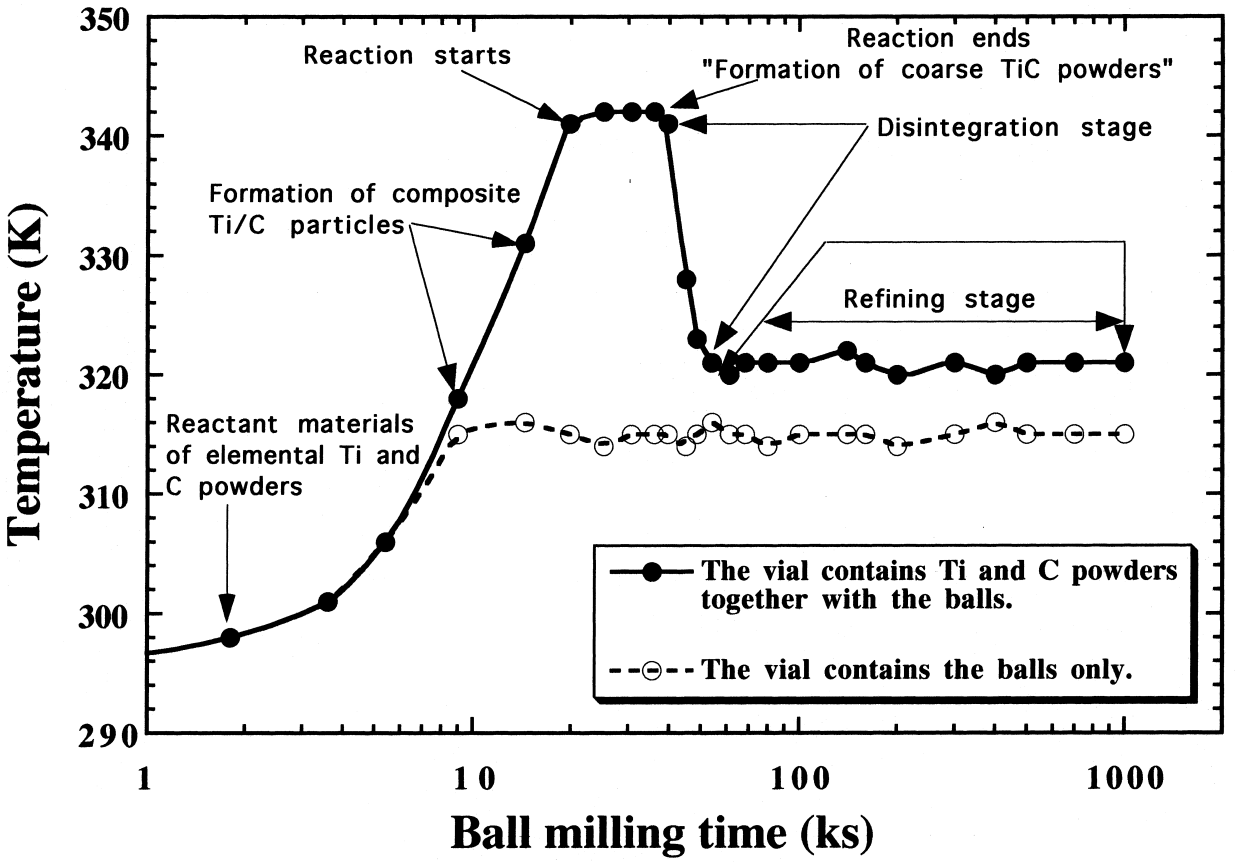

Fig. 18. Dependence of the vial temperature on MA time and vial contents during the ball-milling process (see section 4 in the text).

This final product contains internal extraordinarily fine crystallites of about 4 nm in diameter (Figs. 5 and 6). The temperature of the vial is almost saturated at a value close to 320 K during this last stage of milling that extended from 54 to 1000 ks, as presented in Fig. 18.

4.2. Consolidation of the mechanically alloyed TiC powders

Consolidation of the ball-milled powder is required for most industrial applications. In fact, the sintering step is necessary in order to determine several mechanical and physical properties. Most of the consolidation techniques that are used for sintering the ball-milled powders into compacts, such as HIPing [41], hot pressing [42] and hot extrusion [43], sinter forging [44], usually lead to grain growth. Thus, the sintered powders are either only near fully dense (above 90% of the theoretical density), or fully dense but with grain sizes in the range from sub-micron to several microns. The aim of the present study was to use an effective consolidation process in order to obtain a fully dense, nanocrystalline TiC bulk alloy. Among the several methods of sintering, plasma activated sintering (PAS) is considered one of the most suitable process to obtain fully dense compacts with nano-structured grains [18]. Three important factors govern a successful consolidation step via the PAS. The first factor is the application of a uniaxial load, the second is the application of a pulsed voltage for plasma activation, and the last factor is the resistance heating of graphite crucible and powders. In this consolidation technique, when the direct current pulse voltage is applied to the powders, micro discharge takes place among the TiC particles, which generates a plasma. Hence, the atoms on the surface of each particle are activated, and the sintering procedure takes place in a short time (consolidation is achieved within 0.3 ks). Accordingly, grain growth during sintering can be minimized and the sintered TiC powders (Figs. 11 and 13) maintain their unique nanocrystalline properties with improved physical (Figs. 15) and mechanical properties (Figs. 12,16 and 17). In addition, the PAS technique does not result in any compositional and/or structural changes of the sintered powders. Thus, the as-milled and as-consolidated samples are identical in their properties.

5. Conclusions

Whereas TiC alloys are usually fabricated at high temperatures, the present study demonstrates a powerful technique for preparing single phase TiC with NaCl structure at room temperature. In the present work,

elemental Ti and C powders are milled under argon gas atmosphere using a high-energy ball mill. Single phase of $Ti_{44}C_{56}$ with NaCl structure was obtained after 22 ks of MA time. This carbide phase contains nanocrystalline grains of about 40 nm in diameter. Increasing the MA time to 80 −720 ks results in the formation of ultrafine grains with lens structure morphology of about 5 nm in diameter. This end-product, possessing excellent morphological properties such as homogeneous shape (spherical morphology), fine and smooth surface relief, and uniform size (<0.8 μm in diameter) was consolidated into compact samples using a plasma activated sintering technique. This consolidation step leads to the formation of a fully dense (nearly 100% of the theoretical density) nanocrystalline (with an average grain size of 60 nm) material. The densities, hardness, and some mechanical properties of the consolidated samples were measured as a function of the MA time.

Acknowledgements

The author would like to thank Dr. M. Omori for his kind support during consolidation of the milled powders.

References

[1] H. Gleiter, Prog. Mat. Sci 33 (1990) 4.
[2] H. Hahan, NanoStruct. Mat. 9 (1997) 3.
[3] R. Birringer, H. Gleiter, H.P. Klein, P. Marquardt, Phys. Lett. A 102 (1984) 356.
[4] A. Inoue, Mater. Sci. Eng. A 179/180 (1994) 57.
[5] R.O. Hughes, S.D. Smith, C.S. Pande, H.R. Johnson, R.W. Armstrong, Script. Metall. 20 (1986) 93.
[6] Z.G. Li, D.J. Smith, Appl. Phys. Lett. 55 (1989) 919.
[7] K. Lu, W.D. Wei, J.T. Wang, Script. Metall. Mater. 24 (1995) 2319.
[8] B.H. Kear, P.R. Strutt, NanoStruct. Mat. 6 (1995) 227.
[9] J.S. Benjamin, Met. Trans. 1A (1970) 2943.
[10] W. Sha, Met. Trans. 30A (1999) 1689.
[11] C.C. Koch, O.B. Cavin, C.G. McKamey, J.O. Scarbourgh, Appl. Phys. Lett. 43 (1983) 1017.
[12] R.B. Schwarz, R.R. Petrich, C.K. Saw, J. Non-Cryst. Solids 76 (1985) 281.
[13] P.Y. Lee, C.C. Koch, Appl. Phys. Lett. 50 (1987) 1578.
[14] M. Sherif El-Eskandarany, K. Aoki, K. Suzuki, J. Less-Common Met. 167 (1990) 113.
[15] M. Sherif El-Eskandarany, K. Aoki, K. Suzuki, Appl. Phys. Lett. 70 (1997) 1679.
[16] M. Sherif El-Eskandarany, K. Sumiyama, K. Suzuki, Acta Metall. 36 (1997) 1175.
[17] M. Sherif El-Eskandarany, J. Alloys Compd. 284 (1999) 295.
[18] M. Sherif El-Eskandarany, M. Omori, T.J. Konno, K. Sumiyama, T. Hirai, K. Suzuki, Met. Trans. A 29 (1998) 1973.
[19] Y. Fahmy, T.D. Shen, D.A. Tucker, R.L. Spontak, C.C. Kock, J. Mater. Res. 14 (1999) 2488.
[20] M. Sherif El-Eskandarany, K. Sumiyama, K. Suzuki, J. Mater. Res. 10 (1995) 659.
[21] M. Sherif El-Eskandarany, Met. Trans. A 27 (1996) 2374.
[22] A.A. Mahdy, M. Sherif El-Eskandarany, H.A. Ahmed, A.A. Amer, J. Alloys Compd. 299 (2000) 244–253.
[23] S. Mi, T.H. Courtney, Scripta Metall. 38 (1997) 171.
[24] Ma- Xuaming, Zhao- Ling, Ji- Gang, Dong- Yuanda, J. Rare Metals 17 (1998) 88.
[25] Ma- Xuaming, Zhao- Ling, Ji- Gang, Dong- Yuanda, J. Alloys Compd. 264 (1998) 267.
[26] M. Sherif El-Eskandarany, J. Alloys Compd. 279 (1998) 263.
[27] J.S. Lee, T.H. Kim, J.H. Yu, S.W. Chung, NanoStruct. Mat. 9 (1997) 153.
[28] E.Y. Ivanov, C. Suryanarayana, B.D. Bryskin, Mater. Sci. Eng. A 251 (1998) 255.
[29] C.C. Koch, NanoStruct. Mat. 9 (1997) 13.
[30] E.K. Storms, The Refractory Carbides, Academic Press, New York, 1967.
[31] Xiao-Ming He, Wen-Zhi, Heng-De Li, J. Mater. Res. 9 (1994) 2355.
[32] P. Schwarzkopf, R. Kieffer, Refractory Hard Metals, Macmillan, New York, 1953.
[33] Z.A. Munir, Ceramic. Bull. 67 (1988) 342.
[34] Z.A. Munir, U. Anselmi-Tamburini, Mater. Sci. Rep. 3 (1989) 277.
[35] M. Sherif El-Eskandarany, M. Omori, M. Ishikuro, T.J. Konno, K. Takada, K. Sumiyama, T. Hirai, K. Suzuki, Met. Trans. 26A (1996) 4210.
[36] M. Sherif El-Eskandarany, F. Itoh, K. Aoki, K. Suzuki, J. Non-Cryst. Solids 118 (1990) 729.
[37] M. Sherif El-Eskandarany, K. Aoki, K. Suzuki, J. Appl. Phys. 71 (1992) 2924.
[38] ASTM Card No. 32-1383, ASTM, Philadelphia, PA.M.
[39] A.A. El-Mahdy, M. Sherif El-Eskandarany, H.A. Ahmed, A.A. Amer, J. Alloys Compd. (1999) in press.
[40] F.R. de Boer, R. Boom, W.C.M. Mattens, A.R. Miedema, A.K. Niessen, in: 1st Edition, Cohesion in Metals–Transition Metal Alloys, Vol. 1, North-Holland, Amsterdam, 1988, p. 127.
[41] M. Oehring, F. Appel, Th. Pfullmann, R. Bormann, Appl. Phys. Lett. 66 (1995) 941.
[42] P. Nash, H. Kim, H. Choo, H. Ardy, S.J. Hwang, A.S. Nash, Mater. Sci. Forum 88–99 (1992) 603.
[43] S.J. Hwang, P. Nash, M. Dollar, D. Dymek, Mater. Sci. Forum 88–99 (1992) 611.
[44] M. Jain, T. Christman, Act. Meta. Mater. 42 (1994) 1901.